

# A Parameter Selection Method for Multi-Element Resonant Converters with a Resonant Zero Point

Yifeng Wang<sup>\*</sup>, Liang Yang<sup>†</sup>, Guodong Li<sup>\*\*</sup>, and Shijie Tu<sup>\*\*\*</sup>

<sup>†,\*</sup>Key Laboratory of Smart Grid of the Ministry of Education, Tianjin University, Tianjin, China

<sup>\*\*</sup>State Grid Tianjin Electric Power Company, Tianjin, China

<sup>\*\*\*</sup>Repair Branch, State Grid Jiangxi Electric Power Company, Jiangxi, China

## Abstract

This paper proposes a parameter design method for multi-element resonant converters (MERCs) with a unique resonant zero point (RZP). This method is mainly composed of four steps. These steps include program filtration, loss comparison, 3D figure fine-tuning and priority compromise. It features easy implementation, effectiveness and universal applicability for almost all of the existing RZP-MERCs. Meanwhile, other design methods are always exclusive for a specific topology. In addition, a novel dual-CTL converter is also proposed here. It belongs to the RZP-MERC family and is designed in detail to explain the process of parameter selection. The performance of the proposed method is verified experimentally on a 500W prototype. The obtained results indicate that with the selected parameters, an extensive dc voltage gain is obtained. It also possesses over-current protection and minimal switching loss. The designed converter achieves high efficiencies among wide load ranges, and the peak efficiency reaches 96.9%.

**Key words:** High efficiency, Multi-element resonant converter, Parameter selection, Resonant zero point, Soft-switching

## I. INTRODUCTION

Due to advantages such as high efficiency, low EMI, high power density, the resonant power converters (RPCs) are popular among various applications including the electric vehicle chargers, renewable energy generation and switched mode power supplies [1], [2]. Presently, a large number of studies have been carried out that focus on two-element or three-element RPCs. Among them, the LLC converter, as one of the most advanced three-element RPCs, has been developed in depth. The circuit modelling [3], [4], parameter design [5]-[9], topology morphing [10]-[14], high-frequency performance [15]-[17] and control strategy [18]-[20] have all been investigated. LLC-RPCs harvest higher efficiency and broaden voltage ranges. However, the inherent contradiction between the voltage range and the efficiency is detrimental to the performance of LLC converters.

Fortunately, this problem can be addressed by using MERCs. Generally, a MERC has at least four passive components in the resonant tank. The multi-element characteristic ensures that MERCs have more resonant points than two-element or three-element RPCs. Therefore, this kind of converter exhibits diverse resonant features in different operating frequency ranges. It also shows advantages over the conventional RPCs. Several studies have already conducted research on MERCs, and they successfully improved the conversion performance when compared with traditional RPCs. Nevertheless, due to the complexity of the multiple elements, the parameter selection issue has become an obstacle to the fabrication of MERCs.

Dual-transformer MERCs were discussed in [21]-[27]. In [21]-[23], an auxiliary transformer, often controlled by auxiliary switches, was introduced into a resonant tank. This transformer does not function at the rated state. As result, the MERC operates as a normal LLC converter. Meanwhile, in certain situations, the auxiliary switches enliven the auxiliary transformer to realize different purposes, such as restrained conduction losses, wide voltage ranges and high dc voltage gain. By the same token, the dual-transformer converters in [24], [25] employ two resonant tanks and have successfully obtained desirable features such as low THD and current

Manuscript received May 27, 2017; accepted Oct. 15, 2017  
Recommended for publication by Associate Editor Yan Xing.

<sup>†</sup>Corresponding Author: zyangliang@tju.edu.cn

Tel: +86-022-27406033, Tianjin University

<sup>\*</sup>Key Lab. Smart Grid of Ministry of Education, Tianjin Univ., China

<sup>\*\*</sup>State Grid Tianjin Electric Power Company, China

<sup>\*\*\*</sup>Repair Branch, State Grid Jiangxi Electric Power Company, China

balancing. However, although nearly all of the resonant parameters are selected properly for these MERCs, the relevant design processes are more like those of traditional LLC converters. Hence, they show less instructiveness for MERCs.

Four-element RPCs are another type of MERC and they show considerable merits [28]-[31]. A CLLC converter, reported in [28], achieves a wide voltage range as well as a high efficiency with a peak value of over 98%. It employs a symmetrical structure, where two resonant capacitors and two resonant inductors are pre-set identically and the turns ratio of the transformer is set at 1. This contributes to the simplicity of the parameter design, and results in an attractive symmetry for bidirectional operation. However, the design process also loses representativeness for general MERCs. In [29], a CLCL circuit is designed for a LED driver, in which the switching losses are minimized and high efficiency is guaranteed. The parameters are selected using a simple and effective method through 3D figures. However, the parameter boundaries of the 3D figures are given with no clear motivation. LCLC and LLCC topologies are discussed in [30], [31] for current balancing and parasitic effect elimination. However, some of the parameters are calculated in an intricate mathematic way, while some parameters are given for no obvious reason.

For five-element and higher order RPCs, although more resonant points help the converter in attaining the desirable multi-function characteristic, the difficulty of parameter selection increases progressively. In [32], a five-element LCLCL converter was reported, where its dc voltage gain curve contains four resonant frequency points. Through properly arranging these resonant points, this MERC successfully extends the voltage range, restricts the circulating energy and achieves a desirable over-current protection capability.

The dominant reason that the LCLCL converter is able to possess outstanding performances, can be attributed to its unique RZP. At the RZP, the dc voltage gain is kept zero regardless of load variations. A RZP allows the RPC to modulate the voltage gain flexibly from zero to its maximum value within a narrow frequency range. Consequently, wide voltage ranges can be easily realized. Another benefit from the zero-gain feature is that a RZP-MERC is capable of operating at the RZP for output current restriction, which shows the great merit of the current safeguard. In spite of the many advantages of the RZP-MERC [32]-[35], this kind of converter also suffers due to the intricacy of its parameter selection. In addition, most of the existing RZP-MERCs fail to provide a distinct design process. Some of the selection methods are too specific and not available throughout. With these considerations in mind, a simple, effective and widely applicable parameter design method is of great importance for the RZP-MERCs.

In this paper, a parameter selection method is proposed for RZP-MERCs. A MATLAB-aided program, comprehensive consideration of the conduction losses and turn-off losses, 3D

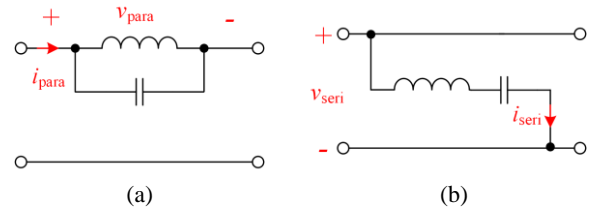


Fig. 1. Two main RZP structures. (a) Parallel type. (b) Series type.

figures selection, and the priorities of the resonant characteristic variables (RCVs) are combined to provide a simple and reliable parameter design method. To facilitate comprehension, a dual-CTL converter with a RZP is taken for an example to explain the proposed method in detail. In addition, the generation mechanism of the RZP is also analyzed. At last, based on a 500W prototype, the designed resonant parameters are tested by experiments. The obtained results demonstrate that the converter achieves a high efficiency, wide voltage gain range and inherent over-current protection.

## II. GENERATION MECHANISM OF THE RESONANT ZERO POINT

This section analyzes the mechanism of RZP converters. Generally, these converters are classified into two types as shown in Fig. 1. These two types are the parallel architectures and the serial architectures. The resonant tank for each of the two types is made up of a resonant capacitor  $C$  and a resonant inductor  $L$ .

For the parallel architecture in Fig. 1(a), the expression of the impedance  $Z_{para}$  is derived as (1), where  $v_{para}$  and  $i_{para}$  are defined as the relevant voltage and current.

$$Z_{para} = \frac{v_{para}}{i_{para}} = \frac{sL}{s^2LC + 1} \quad (1)$$

Substitute  $s = j\omega_s = j2\pi f_s$  into (1), where  $\omega_s$  and  $f_s$  are the operating angular frequency and operating frequency of the converter. Thus, (1) is expressed as:

$$Z_{para} = \frac{j \cdot \omega_s L}{1 - \omega_s^2 LC} \quad (2)$$

From (2), if  $f_s$  reaches a certain frequency as presented in (3), conceptually,  $Z_{para}$  tends to infinite. Thus, the parallel architecture is analogous to the “open circuit” state. The corresponding voltage gain is reduced to and stays at almost zero regardless of load variations. In addition, the converter is operated at the RZP.

$$f_s = \frac{1}{2\pi\sqrt{LC}} \quad (3)$$

The impedance  $Z_{seri}$  of the serial structure in Fig. 1(b) is calculated as:

$$Z_{seri} = \frac{1 - \omega_s^2 LC}{j \cdot \omega_s C} \quad (4)$$

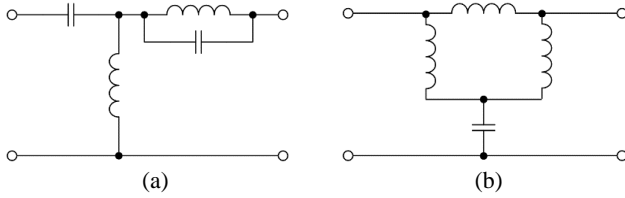


Fig. 2. RZP-MERC topologies: (a) topology 1; (b) topology 2.

Similarly, when (3) is reached,  $Z_{\text{seri}}$  is equal to zero, which means the serial architecture exhibits the “short circuit” characteristic. Consequently, the output voltage is also restricted at zero.

Two RZP-MERCs have been reported in previous studies [24,25], [28] as shown in Fig. 2. This indicates that the RZP-MERC topologies also belong to the parallel or serial architectures as shown in Fig. 1. Hence, each of them possesses a RZP in their voltage gain curves, which provides the benefits of over-current protection and a wide voltage gain. However, the parameter design issue is a big problem for this kind of RPC, since almost all of them have more than three resonant elements. The lack of a universal and practical parameter selection method makes the RZP-MERCs hard to be applied.

### III. PARAMETER SELECTION METHOD

A design block diagram of the proposed parameter selection method is shown in Fig. 3. This method features simplicity, effectiveness and ease of implantation. As a result, it is suitable for RZP-MERCs. The general design procedure includes the following steps:

- 1) Enter the rating dc input voltage  $V_{\text{in}}$ , the output voltage  $V_{\text{out}}$  and the operating frequency  $f_{\text{sr}}$ .
- 2) Establish a first harmonic approximation (FHA) model, and calculate expressions of the dc voltage gain  $M_{\text{gain}}$ , the resonant points and the RZP.
- 3) Confirm the initial ranges and steps of the resonant parameters that need to be selected, and utilize MATLAB to filter these parameters.
- 4) Consider the comprehensive conduction losses and turn-off losses, and confirm the reasonable parameters within narrow ranges.
- 5) Use 3D figures to fine-tune the parameters and determine the optimal parameter range for each separate RCV.
- 6) Set priority for all of the RCVs and compromise to determine the chosen resonant parameters.

Use simulation or experimental results to verify if the design results meet the desired requirements. If it does not, then go to Step 4 and re-select the parameter.

For RZP-MERCs with different architectures, this method is applicable by simply changing the selection constraints of MATLAB. Hence, this method is both effective and practical, and can be applied broadly.

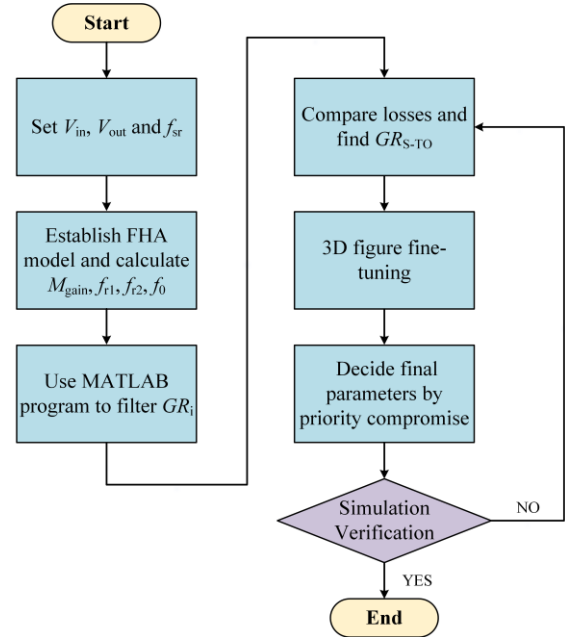


Fig. 3. Block diagram of the proposed parameter design method.

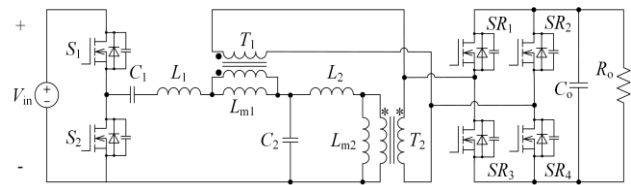


Fig. 4. Topology of the proposed CLTCL converter.

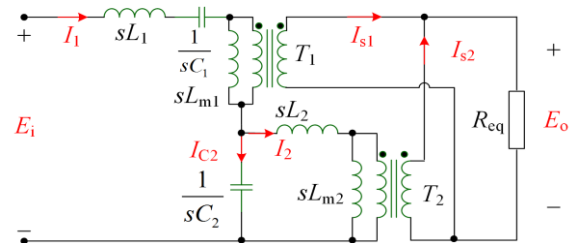


Fig. 5. Equivalent FHA circuit.

To facilitate the explanation of the parameter design method, a dual-CTL RZP converter is taken as an example in the following sections.

### IV. DESIGN EXAMPLE

The topology of the proposed dual-CTL RZP converter is presented in Fig. 4. The resonant tank contains two resonant capacitors  $C_1$  and  $C_2$ , two resonant inductor  $L_1$  and  $L_2$ , and two high frequency transformers  $T_1$  and  $T_2$ . The parallel RZP structure, including  $C_2$ ,  $L_2$  and  $T_2$ , ensures that this topology has a unique RZP  $f_0$ . In addition, the leakage inductors of  $T_1$  and  $T_2$  are integrated into  $L_1$  and  $L_2$ , respectively. As a result, the side effects caused by parasites are also weakened.

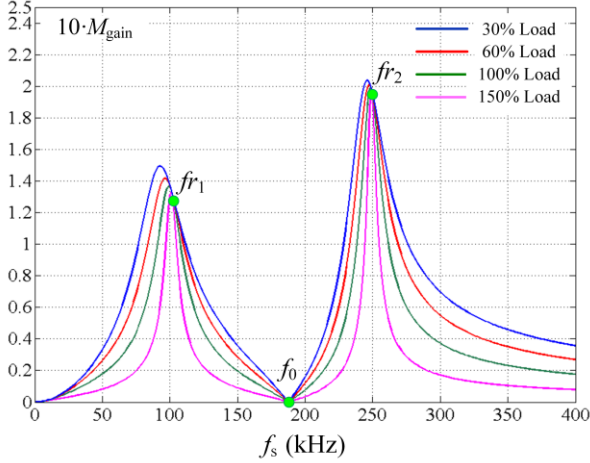


Fig. 6. Voltage gain curves at different loads.

### A. Circuit Modelling

A FHA model of the dual-CLT converter is constructed as shown in Fig. 5.  $E_i$  and  $E_o$  are the fundamental components of the input and output voltages of the resonant tank.  $I_1$ ,  $I_2$  and  $I_{C2}$  are the currents through  $L_1$ ,  $L_2$  and  $C_2$ . In addition,  $I_{S1}$  and  $I_{S2}$  are the secondary currents of  $T_1$  and  $T_2$ . Furthermore,  $R_{eq}$  is the equivalent ac load of the resistor  $R_o$ . Meanwhile,  $V_{T1}$  and  $V_{T2}$  are the primary voltages of  $T_1$  and  $T_2$ . List the KCL / KVL equations as (5), and the dc voltage gain  $M_{gain}$  can be deduced.

$$\begin{cases} E_i = I_1 \cdot (sL_1 + \frac{1}{sC_1}) + V_{T1} + I_2 \cdot sL_2 + V_{T2} \\ I_{C2} \cdot \frac{1}{sC_2} = I_2 \cdot sL_2 + V_{T2} \\ I_1 = I_2 + I_{C2} \\ V_{T1} = N_1 \cdot E_o \\ V_{T2} = N_2 \cdot E_o \\ I_1 = \frac{V_{T1}}{sL_{m1}} + \frac{I_{S1}}{N_1} \\ I_2 = \frac{V_{T2}}{sL_{m2}} + \frac{I_{S2}}{N_2} \\ E_o = R_{eq} \cdot (I_{S1} + I_{S2}) \\ R_{eq} = \frac{8}{\pi^2} R_o \end{cases} \quad (5)$$

Then, based on  $s = j\omega_s$ , where  $\omega_s$  is the relevant angular frequency of the operating frequency  $f_s$ , it is possible to express  $M_{gain}$  as:

$$M_{gain} = \left| \frac{1}{M_{Re} + jM_{Im}} \right| = \left| \frac{1}{(C_\omega + \frac{A_\omega B_\omega}{C_\omega}) + j \frac{A_\omega R_{eq}}{C_\omega}} \right| \quad (6)$$

$$\begin{cases} A_\omega = \omega_s L_1 - \frac{1}{\omega_s C_1} + \frac{\omega_s L_2}{1 - \omega_s^2 C_2 L_2} \\ B_\omega = \frac{N_1^2}{\omega_s L_{m1}} + \frac{N_2^2}{\omega_s L_{m2}} - \frac{\omega_s C_2 N_2^2}{1 - \omega_s^2 C_2 L_2} \\ C_\omega = N_1 + \frac{N_2}{1 - \omega_s^2 C_2 L_2} \end{cases} \quad (7)$$

From (6)-(7), the  $M_{gain}$  curves with different loads are drawn in Fig. 6. This indicates that the dual-CTL converter has two resonant frequency points  $f_{r1}$  and  $f_{r2}$  as well as a RZP  $f_0$ , at which  $M_{gain}$  is kept constant. The converter should be operated within the frequency scope from  $f_{r1}$  to  $f_0$ , where ZVS turning on is guaranteed for the power switches. This narrow range ( $f_{r1}, f_0$ ) also contributes to a broadened voltage gain range.

In addition, from (6), the expressions of the resonant points are calculated as:

$$f_{r1} = \frac{1}{2\pi} \sqrt{\frac{L_1 C_1 + L_2 C_2 + L_2 C_1 - \sqrt{(L_1 C_1 + L_2 C_2 + L_2 C_1)^2 - 4L_1 C_1 L_2 C_2}}{2L_1 C_1 L_2 C_2}} \quad (8)$$

$$f_{r2} = \frac{1}{2\pi} \sqrt{\frac{L_1 C_1 + L_2 C_2 + L_2 C_1 + \sqrt{(L_1 C_1 + L_2 C_2 + L_2 C_1)^2 - 4L_1 C_1 L_2 C_2}}{2L_1 C_1 L_2 C_2}} \quad (9)$$

$$f_0 = \frac{1}{2\pi} \sqrt{\frac{1}{C_2 L_2}} \quad (10)$$

### B. MATLAB Program Filtration

Based on a FHA model, MATLAB is employed to filter the resonant parameters for the first step. From (6)-(10), total of six parameters needs to be selected, including  $C_1$ ,  $C_2$ ,  $L_1$ ,  $L_2$  and the turns ratios  $N_1$  and  $N_2$  of  $T_1$  and  $T_2$ .

Since the secondary sides of  $T_1$  and  $T_2$  are connected in parallel, as shown in Fig. 1, for most of the time, their voltages  $V_{T1}$  and  $V_{T2}$  are clamped by the dc output voltage  $V_{out}$  and do not participate in the resonance. Thus, in this paper, the magnetizing inductors  $L_{m1}$  and  $L_{m2}$  of  $T_1$  and  $T_2$  are chosen for a comprehensive consideration of the circulating energy and the core volume. Small values of  $L_{m1}$  and  $L_{m2}$  increase the transformer losses, while larger values lead to a larger size and a lower power density.

Then, depending on the practical engineering issues, each of these six parameters is given a pre-set wide range. These ranges cover all of the reasonable parameter values. Every variable varies within its given range from the lowest to the highest at a small fixed step. The scopes and steps of these variables are listed in Table I.

Define GR $_i$  ( $i = 1, 2, 3, \dots$ ) as a parameter group. Every GR $_i$  is a combination of the six variables  $\{L_1, L_2, C_1, C_2, N_1, N_2\}$ , and each variable has a certain value. Every GR $_i$  is unique and different from the others. Thus, the GR $_i$  acts as the fundamental element for the following design procedures.

TABLE I  
RANGES AND STEPS FOR THE RESONANT PARAMETERS

Resonant Parameter	Range		Step
Turns Ratios $N_1$	1	8	0.5
Turns Ratios $N_2$	1	8	0.5
Inductor $L_1$	10 $\mu$ H	300 $\mu$ H	10 $\mu$ H
Inductor $L_2$	10 $\mu$ H	300 $\mu$ H	10 $\mu$ H
Capacitor $C_1$	3nF	30nF	3nF
Capacitor $C_2$	3nF	30nF	3nF

MATLAB mainly verifies if a certain  $GR_i$  is consistent with the selection constraints. Group  $GR_{Si}$  ( $i = 1, 2, 3, \dots$ ), which satisfies the constraints, are recorded, while others are automatically abandoned by the program. As a result, all of the satisfactory groups of  $GR_{Si}$  are able to ensure acceptable MERC resonant performances.

The selection constraints for the dual-CTL circuit are listed below.

1)  $f_{r1} < f_0 < f_{r2}$ . Based on (8)-(10), the resonant points should to be arranged properly, so that the  $M_{\text{gain}}$  curves can match well with Fig. 6. The converter achieves a widely adjustable voltage gain within the narrow frequency range from  $f_{r1}$  to  $f_0$ .

2)  $98\text{kHz} < f_{r1} < 102\text{kHz}$ . The rating point  $f_{sr}$  is set at 100kHz. Because  $f_{sr}$  is supposed to closely approach  $f_{r1}$  for loss reduction,  $f_{r1}$  should meet this inequation.

3)  $150\text{kHz} < f_0 < 180\text{kHz}$ . The location of  $f_0$  must be considered carefully, since it is significant for a RZP-MERC. If  $f_0$  is near  $f_{r1}$ ,  $M_{\text{gain}}$  can be modulated flexibly with a small frequency scope. In addition, the circulating energy increases as the detrimental outcomes when  $f_0$  is too closed to  $f_{r1}$ . Hence,  $f_0$  is set among (150kHz, 180kHz) for a compromise [24].

4) Rating voltage gain requirement. To meet the demands of the rating voltages,  $M_{\text{gain}}(f_{r1})$  needs to be designed. Here  $V_{\text{in}} = 400\text{V}$ ,  $V_{\text{out}} = 52\text{V}$ . Thus,  $M_{\text{gain}}(f_{r1})$  is located around 0.13.

5) Leakage inductor requirement. For practical engineering considerations, leakage inductors are generally 3% to 5% of their magnetizing inductors [15]. Hence,  $L_1$  and  $L_2$  must be larger than 5% of  $L_{m1}$  and  $L_{m2}$ , respectively.

A flow chart of MATLAB is shown in Fig. 7. After filtration, the satisfactory groups  $GR_{Si}$  are picked out from the large parameter ranges of Table I to the more limited ranges.

### C. Conduction Loss and Turn-Off Loss

For every  $GR_{Si}$ , the conduction loss and turn-off loss are investigated in this section to determine a trade-off group  $GR_{S\text{-TO}}$ .

The conduction losses are mainly composed of the primary-side loss and the secondary-side loss. For the latter, the square-shape voltage waveform of the SR is exactly in phase with the SR's sine current waveform. This is because the equivalent topology of the SR is altered when its current is equal to zero and flows to the opposite direction. Therefore, the secondary-side conduction loss is positively proportional to the output

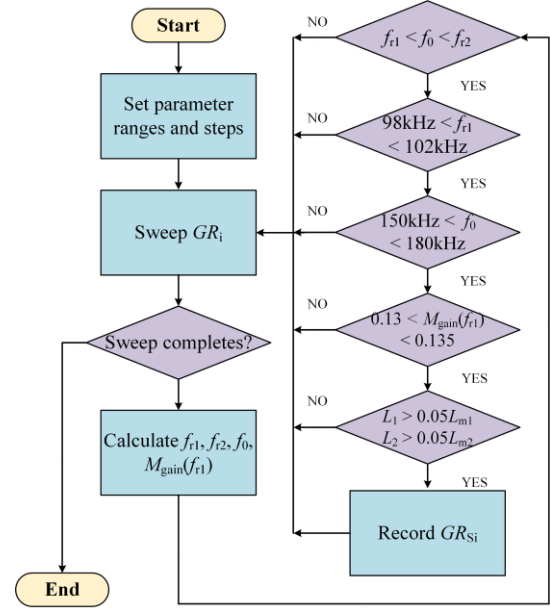


Fig. 7. Flow chart of MATLAB.

current, which is only decided based on the load condition, and has a weak correlation with the resonant parameters. On the other hand, for the primary side, the voltage and current of the resonant tank are not exactly in phase with each other due to the input impedance  $Z_{\text{in}}$ .  $Z_{\text{in}}$  is decided by the resonant tank. Therefore, the relation between the primary-side conduction loss  $P_{\text{conS}}$  and resonant parameters should be analyzed.  $P_{\text{conS}}$  is expressed as (11), where  $T_s$  is the switching period,  $r_{\text{DS}}$  is the conduction resistance of the MOSFET switch and  $i_{S1}(t)$  is the current through  $S_1$ .

$$P_{\text{conS}} = 2 \cdot \frac{1}{2} \cdot \frac{2}{T_s} \int_0^{T_s} r_{\text{DS}} i_{S1}^2(t) dt \quad (11)$$

Based on the FHA analysis, when  $S_1$  turns on, a sinusoidal current can be used to substitute  $i_{S1}(t)$  for the approximation in [6]. Hence, (11) is converted to:

$$P_{\text{conS}} \approx r_{\text{DS}} I_{1\text{-rms}}^2 \quad (12)$$

Where  $I_{1\text{-rms}}$  represents the RMS current of  $L_1$ . From (12), it can be inferred that a smaller  $I_{1\text{-rms}}$  is preferred in order to limit  $P_{\text{conS}}$ .  $I_{1\text{-rms}}$  and  $Z_{\text{in}}$  are deduced as (13)-(15).

$$I_{1\text{-rms}} = \frac{\sqrt{2}V_{\text{in}}}{\pi Z_{\text{in}}} \quad (13)$$

$$Z_{\text{in}} = Z_{\text{Re}} + j \cdot Z_{\text{Im}} \quad (14)$$

$$\begin{cases} Z_{\text{Re}} = \frac{R_{\text{eq}} C_{\omega}^2}{1 + R_{\text{eq}}^2 B_{\omega}^2} \\ Z_{\text{Im}} = A_{\omega} + \frac{R_{\text{eq}}^2 C_{\omega}^2 B_{\omega}}{1 + R_{\text{eq}}^2 B_{\omega}^2} \end{cases} \quad (15)$$

The turn-off loss is dominated by the turn-off current  $I_{\text{turnoff}}$ , which is derived as:

$$I_{\text{turnoff}} = \left| \sqrt{2} I_{1\text{-rms}} \sin(\pi - \varphi_{\text{in}}) \right| = \left| \sqrt{2} I_{1\text{-rms}} \sin(\varphi_{\text{in}}) \right| \quad (16)$$

TABLE II  
PARTIAL SELECTION RESULTS OF MATLAB

$L_1$ ( $\mu\text{H}$ )	$L_2$ ( $\mu\text{H}$ )	$C_1$ (nF)	$C_2$ (nF)	$N_1$	$N_2$	$I_{1\text{-rms}}$ (A)	$\varphi_{\text{in}}$
110	70	12nF	12	1.5	1.5	2.8913	0.83
120	90	9nF	12	2	1	2.8916	0.76
250	90	6	9	2	1	2.8921	0.71
50	60	18	15	1.5	1.5	2.8924	0.74
30	90	15	9	1.5	1.5	2.8928	0.78
200	140	6	6	1.5	1.5	2.8930	0.60
210	50	9	18	2	1	2.8933	0.82
20	220	6	3	1.5	1.5	2.8934	0.71
290	90	6	9	1.5	1.5	2.8938	0.69
80	120	9	9	2	1	2.8940	0.75
60	90	12	12	2	1	2.8943	0.70
70	60	15	18	2	1	2.8946	0.89

Where  $\varphi_{\text{in}}$  is the input impedance angle of the resonant tank.  $\varphi_{\text{in}}$  is

$$\varphi_{\text{in}} = \arctan\left(\frac{Z_{\text{Im}}}{Z_{\text{Re}}}\right) \quad (17)$$

Equation (16) demonstrates that the turn-off loss presents a positive correlation with  $\varphi_{\text{in}}$ . Thus, to limit the turn-off loss,  $\varphi_{\text{in}}$  should be confined. In this case,  $\varphi_{\text{in}}$  at  $f_s = 1.1f_{r1}$  is employed to reflect the turn-off loss for the primary-side switches.

Calculate  $I_{1\text{-rms}}$  and  $\varphi_{\text{in}}$  for each of the  $GR_{S_i}$ . Then, rank the groups, from the group  $GR_{S\text{-LCL}}$  with the lowest  $P_{\text{cons}}$  to the group with the highest  $P_{\text{cons}}$ . Due to a limited article space, only a part of the results is listed in Table II. From this table, the trade-off group  $GR_{S\text{-TO}}$  can be achieved, and the corresponding parameters are listed as  $L_1 = 200\mu\text{H}$ ,  $L_2 = 140\mu\text{H}$ ,  $C_1 = 6\text{nF}$ ,  $C_2 = 6\text{nF}$ ,  $N_1 = 1.5$  and  $N_2 = 1.5$ . Although  $GR_{S\text{-TO}}$  elevates  $I_{1\text{-rms}}$  slightly resulting in a 1% promotion of  $P_{\text{cons}}$ ,  $\varphi_{\text{in}}$  reduces 37% when compared with  $GR_{S\text{-LCL}}$ . This contributes to much lower turn-off losses. Therefore,  $GR_{S\text{-TO}}$  is chosen in this step.

Since the  $GR_{S\text{-TO}}$  has already been decided, the reasonable ranges for the resonant parameters are further confined. Centering on the parameter values of the  $GR_{S\text{-TO}}$ , each of the six resonant parameters is limited within the range from the upper step to the lower step. Nevertheless, the large number of parameters makes it very difficult to conduct the following optimization. Hence, for simplification, some of the parameters are determined first and the remaining parameters are further fine-tuned through 3D figures. By this means, although deviations are inevitably introduced, they can be slight and negligible due to the very limited parameter scopes. Here, the parameters of the transformers are preset. At the same time, the ranges for the remaining parameters are obtained as:  $L_1$  ( $200\mu\text{H} \pm 10\mu\text{H}$ ),  $L_2$  ( $140\mu\text{H} \pm 10\mu\text{H}$ ),  $C_1$  ( $6\text{nF} \pm 3\text{nF}$ ) and  $C_2$  ( $6\text{nF} \pm 3\text{nF}$ ).

#### D. 3D Figure Fine-Tuning

The 3D figures are drawn according to the deduced expressions of different RCVs, including  $\varphi_{\text{in}}$ ,  $M_{\text{gain}}$  and the ac

voltage stresses  $V_{C1}$  and  $V_{C2}$  of the capacitor  $C_1$  and  $C_2$ . These 3D figures reflect the variation trends between the RCVs and the resonant parameters. Since the borders of these figures were determined at the end of Part C, the main objective of this step is to fine-tune the parameters.

From the  $\varphi_{\text{in}}$  aspect, on one hand,  $\varphi_{\text{in}}$  must keep above zero for ZVS operation. On the other hand,  $\varphi_{\text{in}}$  is supposed to be closed enough to zero so that the turn-off current is limited and the primary-side switches achieve quasi-ZCS turning off.

For  $M_{\text{gain}}$ , since  $M_{\text{gain}}(f_{r1})$  is located at around 0.13, the  $M_{\text{gain}}$  of the rating point  $f_{\text{sr}}$  should be equal to or above 0.13 in consideration of the rating voltages. In addition, the varying slope of  $M_{\text{gain}}$  is expected to be mild to weaken the impacts brought by parasites.

Taking the ac voltage stresses into consideration, both  $V_{C1}$  and  $V_{C2}$  must be restricted. In addition, from (5),  $V_{C1}$  and  $V_{C2}$  are derived as:

$$V_{C1} = \left| \sqrt{2}E_1 \cdot \frac{V_{C1\text{-Re1}} + j \cdot V_{C1\text{-Im1}}}{V_{C1\text{-Re2}} + j \cdot V_{C1\text{-Im2}}} \right| \quad (18)$$

$$V_{C2} = \left| \sqrt{2}E_1 \cdot \frac{V_{C2\text{-Re1}} + j \cdot V_{C2\text{-Im1}}}{V_{C2\text{-Re2}} + j \cdot V_{C2\text{-Im2}}} \right| \quad (19)$$

$$\begin{cases} V_{C1\text{-Re1}} = 1 \\ V_{C1\text{-Im1}} = -R_{\text{eq}} B_{\omega} \\ V_{C1\text{-Re2}} = -\omega_s C_1 A_{\omega} \\ V_{C1\text{-Im2}} = \omega_s R_{\text{eq}} C_1 (A_{\omega} B_{\omega} + C_{\omega}^2) \end{cases} \quad (20)$$

$$\begin{cases} V_{C2\text{-Re1}} = R_{\text{eq}} (A_{\omega} B_{\omega} + B_{\omega} \frac{1 - \omega_s^2 L_1 C_1}{\omega_s C_1} + C_{\omega}^2 - N_1 C_{\omega}) \\ V_{C2\text{-Im1}} = A_{\omega} + \frac{1 - \omega_s^2 L_1 C_1}{\omega_s C_1} \\ V_{C2\text{-Re2}} = R_{\text{eq}} C_1 (A_{\omega} B_{\omega} + C_{\omega}^2) \\ V_{C2\text{-Im2}} = A_{\omega} \end{cases} \quad (21)$$

Before drawing the 3D figures, the evaluation of  $C_2$  is implemented. From equation (10) it can be known that the RZP  $f_0$  is mainly decided by  $C_2$  and  $L_2$ .  $f_0$  is of great significance for a RZP-MERC, since it directly influences the voltage gain range and the operating frequency scope. Thus,  $f_0$  should be in accordance with inequation (3) as analyzed above. However, concerning a small value of  $C_2$ , a slight variation of  $C_2$  leads to a large deviation of  $f_0$ . When  $C_2$  varies by 1nF, a 11% deviation of  $f_0$  occurs. Meanwhile when  $L_2$  changes by  $10\mu\text{H}$ , only a 5.6% deviation is generated. This phenomenon is illustrated in Fig. 8, where  $M_{\text{gain}}$  curves are drawn at  $C_2 = 4.5\text{nF}$ ,  $3\text{nF}$ . The corresponding RZPs are located at 217kHz and 265kHz, and they both contradict with inequation (3). Under this condition, the proposed converter loses the attractive over-current protection and widely adjustable voltage gain within a narrow frequency band. As a consequence, to avoid

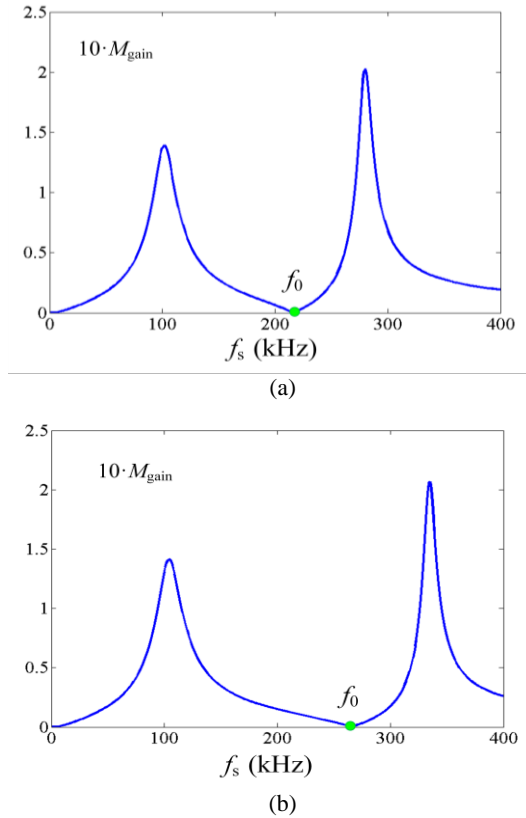


Fig. 8. RZP positions for different values of  $C_2$ : (a)  $C_2 = 4.5 \text{ nF}$ ; (b)  $C_2 = 3 \text{ nF}$ .

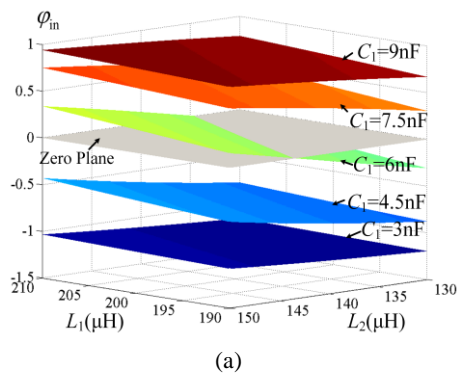


TABLE III  
OPTIMIZED PARAMETERS AND PRIORITIES

Objective	Optimized Parameters	Priority
Impedance angle $\varphi_{\text{in}}$	$C_1$ sets at 6nF	1
	$L_1$ is from 190 $\mu\text{H}$ to 200 $\mu\text{H}$	
	$L_2$ is from 145 $\mu\text{H}$ to 150 $\mu\text{H}$	
Voltage gain $M_{\text{gain}}$	$C_1$ is from 5nF to 7nF	2
Voltage Stress $V_{C1}$	Small $L_1$	3
	$C_1$ is not within (5nF, 7nF)	
Voltage Stress $V_{C2}$	Small $L_2$	4
	$C_1$ is not within (5nF, 7nF)	

TABLE IV  
LIST OF OPTIMIZED PARAMETERS

Parameter	Value
Magnetic inductor $L_{m1}$	300 $\mu\text{H}$
Turns ratio $N_1$	1.5:1
Magnetic inductor $L_{m2}$	300 $\mu\text{H}$
Turns ratio $N_2$	1.5:1
Inductor $L_1$	190 $\mu\text{H}$
Inductor $L_2$	145 $\mu\text{H}$
Capacitor $C_1$	6nF
Capacitor $C_2$	6nF
Rated operating frequency $f_{sr}$	100kHz
Rated load $R_o$	5.4 $\Omega$

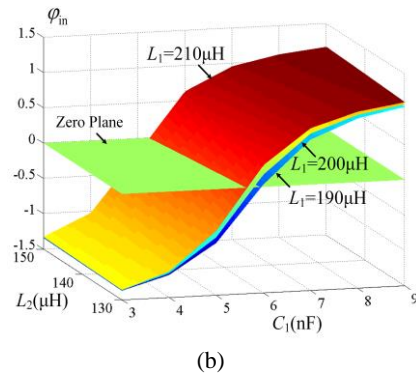


Fig. 9. Relations of  $\varphi_{\text{in}}$  and the resonant parameters. (a)  $\varphi_{\text{in}}$  versus  $L_1$  and  $L_2$  at different values of  $C_1$ . (b)  $\varphi_{\text{in}}$  versus  $C_1$  and  $L_2$  at different values of  $L_1$ .

a large deviation of  $f_0$ , the value of  $C_2$  is fixed at 6nF, which simplifies the following processes.

The relations between  $\varphi_{\text{in}}$  and the resonant parameters  $L_1$ ,  $L_2$  and  $C_1$  are shown in Fig. 9. In Fig. 9a, five surfaces corresponding to  $C_1$  from 3nF to 9nF are presented. Since  $\varphi_{\text{in}}$  needs to be above and closed to zero for ZVS operation and low turn-off losses, the demand is only satisfied when  $C_1$  is 6nF,  $L_2$  is from 145 $\mu\text{H}$  to 150 $\mu\text{H}$ , and  $L_1$  is from 190 $\mu\text{H}$  to 200 $\mu\text{H}$ . Meanwhile, Fig. 9b illustrates the relation of  $\varphi_{\text{in}}$  versus various values of  $L_1$ .  $\varphi_{\text{in}}$  is kept lower than zero unless  $C_1$  is higher than 6nF, and no obvious relation between  $\varphi_{\text{in}}$  and  $L_1$  is found. Thus, in terms of the above analyses, for  $\varphi_{\text{in}}$  alone,  $C_1$

should be set at 6nF, and  $L_1$  and  $L_2$  are expected to be located within (190 $\mu\text{H}$ , 200 $\mu\text{H}$ ) and (145 $\mu\text{H}$ , 150 $\mu\text{H}$ ).

Fig. 10 shows  $M_{\text{gain}}$  curves versus  $L_1$ ,  $L_2$  and  $C_1$ . It is clearly shown that  $M_{\text{gain}}$  reaches its peak values around 0.13 in the scope from 5nF to 7nF. In addition, there are less clues indicating the correlations between  $M_{\text{gain}}$  and  $L_1$  &  $L_2$ . As a result, the  $C_1$  range of 5nF to 7nF is preferred in consideration of  $M_{\text{gain}}$ .

From the voltage stress aspect, the  $V_{C1}$  and  $V_{C2}$  curves versus  $L_1$ ,  $L_2$  and  $C_1$  are shown in Fig. 11 and Fig. 12, respectively.  $V_{C1}$  and  $V_{C2}$  both reach their peaks during the  $C_1$  range of 5nF to 7nF. For  $V_{C1}$ , it rises along with the augment of  $L_1$ , and has

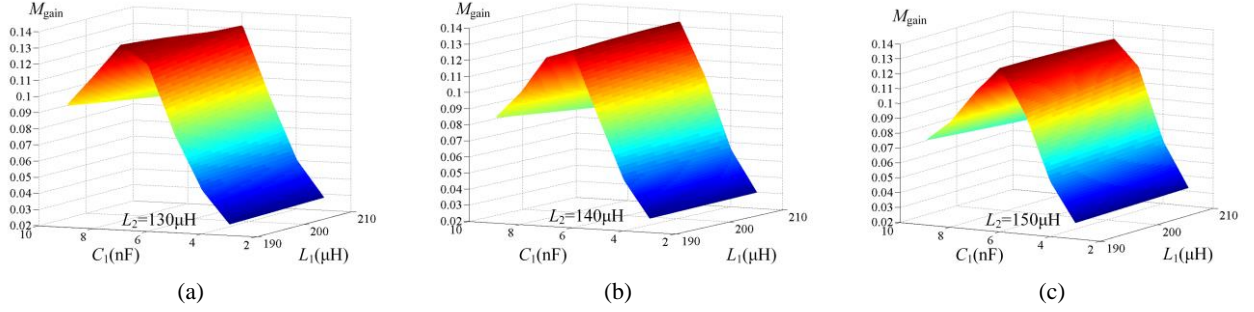


Fig. 10. Relationships of  $M_{\text{gain}}$  and the resonant parameters. (a)  $L_2 = 130\mu\text{H}$ . (b)  $L_2 = 140\mu\text{H}$ . (c)  $L_2 = 150\mu\text{H}$ .

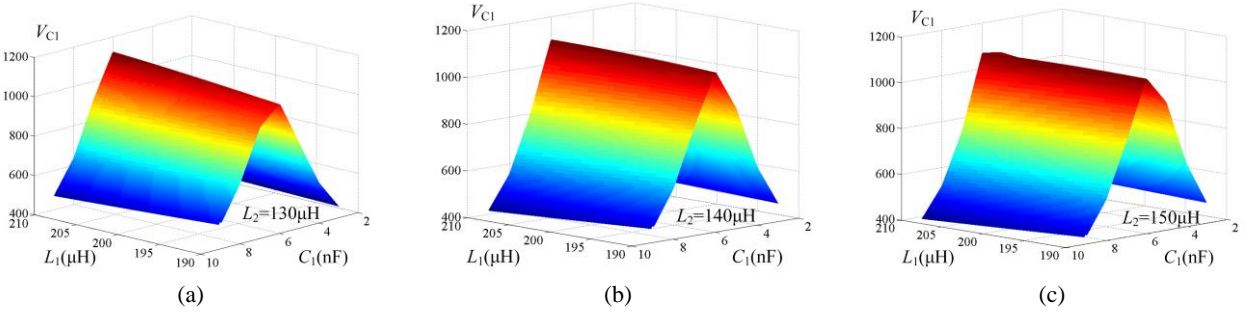


Fig. 11. Relationships of  $V_{C1}$  and the resonant parameters. (a)  $L_2 = 130\mu\text{H}$ . (b)  $L_2 = 140\mu\text{H}$ . (c)  $L_2 = 150\mu\text{H}$ .

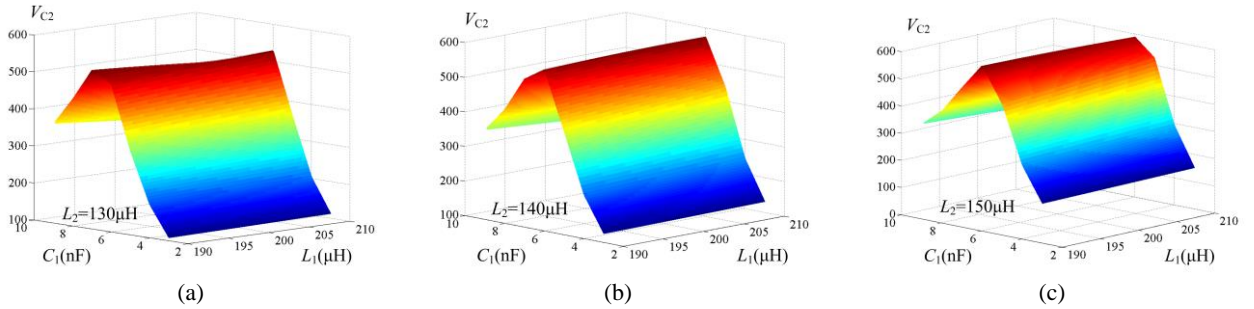


Fig. 12. Relationships of  $V_{C2}$  and the resonant parameters. (a)  $L_2 = 130\mu\text{H}$ . (b)  $L_2 = 140\mu\text{H}$ . (c)  $L_2 = 150\mu\text{H}$ .

weak correlation with variations of  $L_2$ . Similarly,  $V_{C2}$  shows a positive relation with  $L_2$ , and it is barely influenced by  $L_1$ .

### E. Priorities for RCVs

To conclude the 3D figures, for each RCV, and an optimal parameter range can be found without concerning other RCVs. Unfortunately, it is impossible to meet all of the demands of the RCVs synchronously, since these optimal ranges may contradict with each other. Accordingly, to deal with this problem, the priority for each of the RCVs is taken into account. The RCV with a higher priority ought to be satisfied at first, since it is more important when compared with the other RCVs. The optimal parameter ranges and priorities for all of the RCVs are listed in Table. III.

$\varphi_{\text{in}}$  has the highest priority since the efficiency issue is of the most importance for dual-CTL converters. Meanwhile,  $\varphi_{\text{in}}$  represents the dominant influence on the ZVS turn-on and the quasi-ZCS turn-off losses for the primary-side switches.  $M_{\text{gain}}$  has the second highest priority, since the rating input and

output voltages must be set appropriately. The priorities of the voltage stresses are lower since by applying advanced switching devices with higher withstand voltages, high voltage stresses can be tolerated despite the rising costs.  $V_{C1}$  is much higher than  $V_{C2}$ . Therefore, the former ranks higher. At last, concerning Table III, the final resonant parameters are selected and listed in Table. IV.

## V. EXPERIMENTS

To verify the practicability of the proposed design method, a 500W dual-CTL prototype was fabricated in the laboratory. Key waveforms and efficiency conditions are tested experimentally.

Fig. 13 presents waveforms under the rating situation, where the voltage  $v_{S1}$  and current  $i_{S1}$  of the switch  $S_1$ , and the voltage  $v_{SR1}$  and current  $i_{SR1}$  of the SR switch  $SR_1$  are given. Fig. 13(a) indicates that with the chosen parameters, the input impedance angle  $\varphi_{\text{in}}$  is confined to a small value above zero.  $i_{S1}$  lags almost



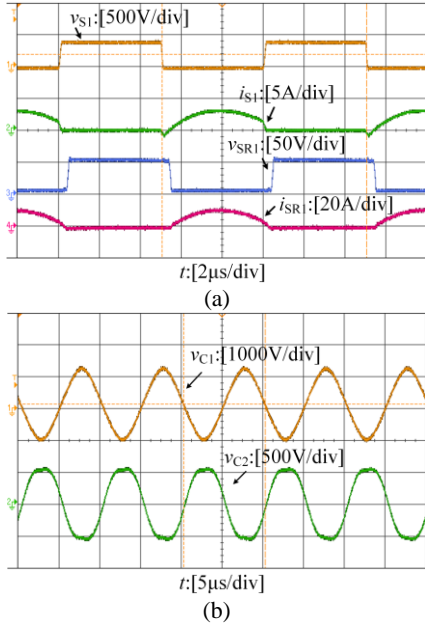


Fig. 13. Waveforms at the rating condition: (a) voltages and currents of  $S_1$  and  $SR_1$ ; (b) voltages of  $C_1$  and  $C_2$ .

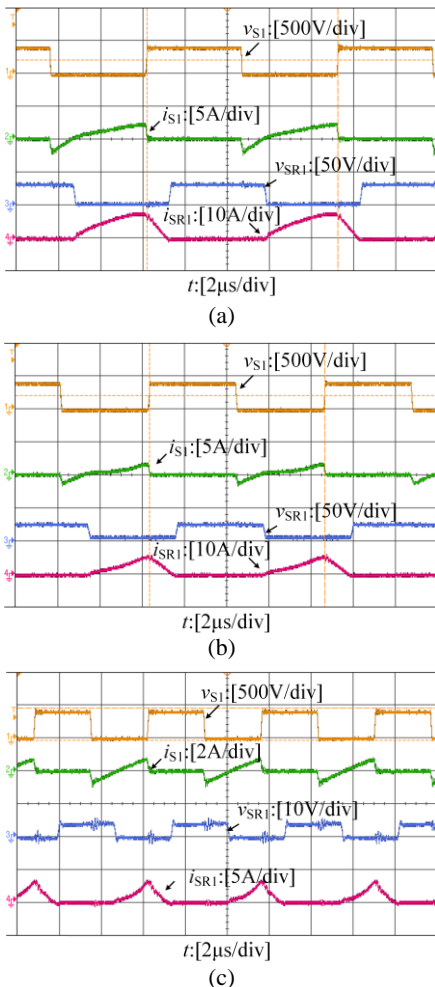


Fig. 14. Waveforms at different operating frequencies: (a)  $f_s = 110\text{kHz}$ ; (b)  $f_s = 140\text{kHz}$ ; (c)  $f_s \approx f_0 = 183\text{kHz}$ .

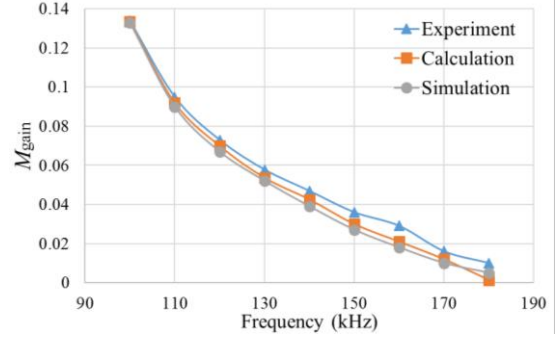


Fig. 15. Comparison of  $M_{gain}$  curves.

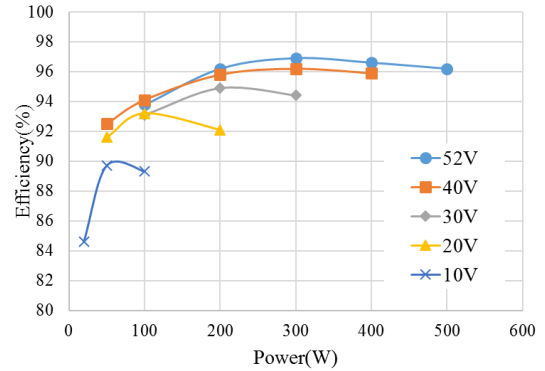


Fig. 16. Efficiency curves with different output voltages.

half a switching cycle behind  $v_{S1}$ , which infers the  $i_{S1}$  is nearly in phase with the drive signal of  $S_1$ . In addition,  $S_1$  fulfills the ZVS turning on and the quasi-ZCS turn-off, since  $i_{S1}$  resonates to almost zero when  $S_1$  is turned off. At the same time,  $SR_1$  maintains its inherent ZCS turn-off, and achieves quasi-ZCS turning on due to the small turn-on current. Accordingly, the switching losses is minimized, which contributes to highly efficient conversions.

The voltages across  $C_1$  and  $C_2$  are shown in Fig. 13(b) as  $v_{C1}$  and  $v_{C2}$ .  $v_{C1}$  is made up of two parts. The two parts are a dc component, which is equal to half of the input voltage  $V_{in}$ , and an ac component, whose amplitude is  $V_{C1}$ .  $V_{C1}$  is measured as 1106V and calculated as 1080.9V from (19). The amplitude  $V_{C2}$  of  $v_{C2}$  is measured as 522V and calculated as 558V. The deviation of  $V_{C2}$  is caused by the distortion of  $v_{C2}$ .

Waveforms at different operating frequencies are given in Fig. 14, where the input voltage  $V_{in}$  is rated at 400V. In Fig. 14(a) and 14(b),  $f_s$  is set at 110kHz and 140kHz, respectively. In addition, the corresponding output voltages are 37.2V and 18.3V.  $\phi_{in}$  increases because  $f_s$  is away from the rating point  $f_{sr}$ .  $S_1$  loses the quasi-ZCS but still possesses the ZVS turning on.  $SR_1$  maintains the quasi-ZCS turn-on and ZCS turn-off soft-switching.

In Fig. 14(c), with the rating input voltage, the output voltage is only 4.1V at  $f_s = 183\text{kHz}$ . The voltage gain  $M_{gain}$  is around 0.01. Therefore, this frequency is regarded as the RZP  $f_0$ . It ensures that the dual-CTL converter possesses the inherent over-current protection and the widely adjustable voltage gain.

The calculations, simulations and experiment results of the dc voltage gain curves are compared in Fig. 15. It can be clearly seen that the three curves basically match each other from  $f_{r1}$  to  $f_0$ . When  $f_s$  approaches  $f_{sr}$ , these curves almost converge to a single point. Meanwhile, when  $f_s$  is near  $f_0$ , small deviation occurs. This deviation is caused by the intrinsic error of the FHA analysis and parasitic parameters. Fig. 15 shows that the proposed parameter design method has excellent accuracy.

Efficiency curves with the rating input voltage and different output voltages are given in Fig. 16. Under the rated condition where  $V_{out} = 52V$ , the efficiency is at its highest, and the peak value is 96.9% at 300W. This higher efficiency, when compared with similar high step-down RPCs [16], [18], [20], verifies the effectiveness of the designed dual-CTL converter. For other operating states, the efficiency curves inevitably drop due to deviations from the rating point. Despite of this, the converter still maintains a relatively high efficiencies for a wide voltage gain range.

## VI. CONCLUSIONS

A parameter selection method is proposed for RZP-MERCs in this paper. The main objective of this method is to narrow the acceptable range for all of the variables. Through MATLAB, loss comparisons and 3D figures, the first three steps seek out reasonable parameters within very limited scopes. Then, the last step determines the final resonant parameters by a priority compromise. For different topologies, by altering the selection constraints in the program, it is easy to implant this method on most of the current RZP-MERCs. In addition, a novel dual-CTL MERC is taken as an example to explain the design process. A 500W prototype is established to test the performance. Experiments verify that the proposed converter harvests a wide voltage gain range, limited switching loss, over-current protection and a relatively high efficiency along the entire load range.

## REFERENCES

- [1] C. S. Wang, W. Li, Y. F. Wang, F. Q. Han, Z. Meng, and G. D. Li, "An isolated three-port bidirectional DC-DC converter with enlarged ZVS region for HESS applications in DC microgrids," *Energies*, Vol. 10, No. 4, 446, Apr. 2017.
- [2] J. H. Han and Y. C. Lim, "Design of an LLC resonant converter for driving multiple LED lights using current balancing of capacitor and transformer," *Energies*, Vol. 8, No. 3, pp. 2125-2144, Mar. 2015.
- [3] S. Tian, F. C. Lee, and Q. Li, "A simplified equivalent circuit model of series resonant converter," *IEEE Trans. Power Electron.*, Vol. 31, No. 5, pp. 3922-3931, May 2016.
- [4] S. Hu, X. Li, M. Lu, and B. Y. Luan, "Operation modes of a secondary-side phase-shifted resonant converter," *Energies*, Vol. 8, No. 11, pp. 12314-12330, Oct. 2015.
- [5] R. Beiranvand, B. Rashidian, M. R. Zolghadri, and S. M. H. Alavi, "Optimizing the normalized dead-time and maximum switching frequency of a wide-adjustable-range LLC resonant converter," *IEEE Trans. Power Electron.*, Vol. 26, No. 2, pp. 462-472, Feb. 2011.
- [6] R. Beiranvand, B. Rashidian, M. R. Zolghadri, and S. M. H. Alavi, "A Design procedure for optimizing the LLC resonant converter as a wide output range voltage source," *IEEE Trans. Power Electron.*, Vol. 27, No. 8, pp. 3749-3763, Aug. 2012.
- [7] R. Yu, G. K. Y. Ho, B. M. H. Pong, B. W. K. Ling, and J. Lam, "Computer-aided design and optimization of high-efficiency LLC series resonant converter," *IEEE Trans. Power Electron.*, Vol. 27, No. 7, pp. 3243-3256, Jul. 2012.
- [8] X. Fang, H. Hu, F. Chen, U. Somani, E. Auadisiyan, J. Shen, and I. Batarseh, "Efficiency-oriented optimal design of the LLC resonant converter based on peak gain placement," *IEEE Trans. Power Electron.*, Vol. 28, No. 5, pp. 2285-2296, May 2013.
- [9] J. Tian, J. Gao, and Y. Zhang, "Design of a novel integrated L-C-T for PSFB ZVS converters," *J. Power Electron.*, Vol. 17, No. 4, pp. 905-913, Jul. 2017.
- [10] J. W. Kim, J. W. Kim, and G. W. Moon, "A new LLC series resonant converter with a narrow switching frequency variation and reduced conduction losses," *IEEE Trans. Power Electron.*, Vol. 29, No. 8, pp. 4278-4287, Aug. 2014.
- [11] Y. Gu, Z. Lu, L. Hang, Z. Qian, and G. Huang, "Three level LLC series resonant DC/DC converter," *IEEE Trans. Power Electron.*, Vol. 20, No. 4, pp. 781-789, Jul. 2005.
- [12] H. Wu, T. Xia, X. Zhan, P. Xu, and Y. Xing, "Resonant converter with resonant-voltage-multiplier rectifier and constant-frequency phase-shift control for isolated buck-boost power conversion," *IEEE Trans. Ind. Electron.*, Vol. 62, No. 11, pp. 6974-6985, Nov. 2015.
- [13] T. Jiang, J. Zhang, X. Wu, K. Sheng, and Y. Wang, "A bidirectional LLC resonant converter with automatic forward and backward mode transition," *IEEE Trans. Power Electron.*, Vol. 30, No. 2, pp. 757-770, Feb. 2015.
- [14] J. Wu, Y. Li, X. Sun, and F. Liu, "A new dual-bridge series resonant DC-DC converter with dual-tank," *IEEE Trans. Power Electron.*, to be published.
- [15] Y. Guan, Y. Wang, D. Xu, and W. Wang, "A 1 MHz half-bridge resonant DC/DC converter based on GaN FETs and planar magnetics," *IEEE Trans. Power Electron.*, Vol. 32, No. 4, pp. 2876-2891, Apr. 2017.
- [16] M. Mu and F. C. Lee, "Design and optimization of a 380-12V high-frequency, high-current LLC converter with GaN devices and planar matrix transformers," *J. Emerg. Sel. Topics Power Electron.*, Vol. 4, No. 3, pp. 854-862, Sep. 2016.
- [17] W. Lee, D. Han, C. T. Morris, and B. Sarlioglu, "High-frequency GaN HEMTs based point-of-load synchronous buck converter with zero-voltage switching," *J. Power Electron.*, Vol. 17, No. 3, pp. 601-609, May 2017.
- [18] N. Shafiei, M. Ordonez, M. Craciun, C. Botting, and M. Edington, "Burst mode elimination in high-power LLC resonant battery charger for electric vehicles," *IEEE Trans. Power Electron.*, Vol. 31, No. 2, pp. 1173-1188, Feb. 2016.
- [19] J. H. Kim, C. E. Kim, J. K. Kim, J. B. Lee, and G. W. Moon, "Analysis on load-adaptive phase-shift control for high efficiency full-bridge LLC resonant converter under light-load conditions," *IEEE Trans. Power Electron.*, Vol.

- 31, No. 7, pp. 4942-4955, Jul. 2016.
- [20] J. Jang, S. K. Pidarparthy, and B. Choi, "Current mode control for LLC series resonant DC-to-DC converters," *Energies*, Vol. 8, No. 6, pp. 6098-6113, Jun. 2015.
- [21] M. T. Outeiro, G. Buja, and D. Czarkowski, "Resonant power converters: an overview with multiple elements in the resonant tank network," *IEEE Ind. Electron. Mag.*, Vol. 10, No. 2, pp. 21-45, Jun. 2016.
- [22] H. Hu, X. Fang, F. Chen, Z. J. Shen, and I. Batarseh, "A modified high-efficiency LLC converter with two transformers for wide input-voltage range applications," *IEEE Trans. Power Electron.*, Vol. 28, No. 4, pp. 1946-1960, Jul. 2013.
- [23] Z. Liang, R. Guo, J. Li, and A. Q. Huang, "A high-efficiency PV module-integrated DC/DC converter for PV energy harvest in FREEDM systems," *IEEE Trans. on Power Electron.*, Vol. 26, No. 3, pp. 897-909, Mar. 2011.
- [24] C. C. Hua, Y. H. Fang, and C. W. Lin, "LLC resonant converter for electric vehicle battery chargers," *IET Power Electron.*, Vol. 9, No. 12, pp. 2369-2376, Jul. 2016.
- [25] Y. Du and A. K. S. Bhat, "Analysis and design of a high-frequency isolated dual-tank LCL resonant AC-DC converter," *IEEE Trans. Ind. Appl.*, Vol. 52, No. 2, pp. 1566-1576, Mar./Apr. 2016.
- [26] C. Wang, L. Yang, Y. Wang, and B. Chen, "A 1kW CLTCL resonant DC-DC converter with restricted switching loss and broadened voltage range," *IEEE Trans. Power Electron.*, to be published.
- [27] H. Wu, X. Zhan, and Y. Xin, "Interleaved LLC resonant converter with hybrid rectifier and variable-frequency plus phase-shift control for wide output voltage range applications," *IEEE Trans. Power Electron.*, Vol. 32, No. 6, pp. 4246-4257, Jun. 2017.
- [28] J. H. Jung, H. S. Kim, M. H. Ryu, and J. W. Baek, "Design methodology of bidirectional CLLC resonant converter for high-frequency isolation of DC distribution systems," *IEEE Trans. Power Electron.*, Vol. 28, No. 4, pp. 1741-1755, Apr. 2013.
- [29] Y. Wang, Y. Guan, D. Xu, and W. Wang, "A CLCL resonant DC/DC converter for two-stage LED driver system," *IEEE Trans. Ind. Electron.*, Vol. 63, No. 5, pp. 2883-2891, May 2016.
- [30] X. Qu, S. C. Wong, and C. K. Tse, "An improved LCLC current-source-output multistring LED driver with capacitive current balancing," *IEEE Trans. Power Electron.*, Vol. 30, No. 10, pp. 5783-5791, Oct. 2015.
- [31] J. H. Cheng and A. F. Witulski, "Analytic solutions for LLC parallel resonant converter simplify use of two- and three-element converters," *IEEE Trans. Power Electron.*, Vol. 13, No. 2, pp. 235-243, Mar. 1998.
- [32] D. Fu, F. C. Lee, Y. Liu, and M. Xu, "Novel multi-element resonant converters for front-end dc/dc converters," in *Proceedings of the IEEE Power Electronics Specialists Conference*, pp. 250-256, 2008.
- [33] J. Koscelnik, M. Prazenica, M. Frivaldsky, and S. Ondirko, "Design and simulation of multi-element resonant LCTL converter with HF transformer," in *Proceedings of the ELEKTRO*, pp. 307-311, 2014.
- [34] T. Mishima, H. Mizutani, and M. Nakaoka, "Experimental evaluations of a five-element multi-resonant dc-dc converter with an improved PFM control range," in *Proceedings of*

*the IEEE International Conference Power Electronics and Drive Systems*, pp. 147-152, 2013.

- [35] H. Wu, X. Jin, H. Hu, and Y. Xing, "Multielement resonant converters with a notch filter on secondary side," *IEEE Trans. Power Electron.*, Vol. 31, No. 6, pp. 3999-4004, Jun. 2016.
- [36] D. Huang, F. C. Lee, and D. Fu, "Classification and selection methodology for multi-element resonant converters," in *Proceedings of the 26th Annual IEEE Applied Power Electronics Conference and Exposition*, pp. 558-565, 2011.



**Yifeng Wang** was born in Hubei, China, in 1981. He received his B.S., M.S. and Ph.D. degrees in Electrical Engineering from the Harbin Institute of Technology, Harbin, China, in 2005, 2007 and 2011, respectively. Since 2011, he has been an Associate Professor in the Department of Electrical and Electronics Engineering, Tianjin University,

Tianjin, China. His current research interests include the high frequency and soft-switching power converters used for special power supplies, EV chargers, residential photovoltaic grid-connected generation systems, distributed smart wind power generation systems, and the application of power conversion technology to hybrid AC/DC microgrids.



**Liang Yang** was born in Henan, China, in 1989. He received his B.S. degree in Electrical Engineering from Tianjin University, Tianjin, China, in 2013, where he is presently working towards his Ph.D. degree in Electrical Engineering. His current research interests include small-scale wind generation and high frequency planar

magnetic based DC-DC converters.



**Guodong Li** was born in 1978. He received his B.S. degree in Electrical Engineering from the Northeast Electric Power University, Jilin City, China; and his M.S. degrees in Electrical Engineering from Tianjin University, Tianjin, China. His current research interests include new energy grid-connected detection technologies.



**Shijie Tu** was born in Jiangxi, China, in 1991. He received his B.S. degree in Electrical Engineering from Tianjin University, Tianjin, China, in 2013. His current research interests include DC-DC converters.